

Data-efficient and Safe Learning for Locomotion using a Simplified Model

Junhyeok Ahn¹, Jaemin Lee¹, and Luis Sentis^{2†}

Abstract—In this letter, we formulate a novel Markov Decision Process (MDP) for safe and data-efficient learning for locomotion via a simplified model. In our previous studies of biped locomotion, we relied on a low-dimensional robot model, commonly used in high-level Walking Pattern Generators (WPGs). However, a low-level feedback controller cannot precisely track desired footstep locations due to the discrepancies between the real system and the simplified model. In this study, we propose to mitigate this problem by complementing the WPG with reinforcement learning. We formulate an MDP that incorporates the dynamic properties of a robot, desired walking directions, and footstep features. Safely and efficiently, we iteratively update a policy that determines footstep locations using a simplified model. The footstep policy of the proposed approach consists of the simple-model-based action and a parameterized stochastic action. In addition, a control barrier function process applies corrections to the above policy to prevent exploration of unsafe regions during learning. Our contributions include (1) learning-based compensation for footstep tracking errors resulting from employing the simplified model, (2) efficient and safe exploration in the learning process, and (3) scalability of the procedure to various humanoid robots.

I. INTRODUCTION AND RELATED WORK

Humanoid robots are advantageous for mobility in tight spaces. However, fast bipedal locomotion requires precision control of the contact transition process. Many studies have successfully addressed agile and versatile legged locomotion. Analytic approaches have employed differential dynamics of robots to synthesize locomotion controllers. Data-driven have approached leverage the representational power of neural networks and design locomotion policies. Our work combines the advantages of these approaches to achieve locomotion behaviors safely and efficiently.

Analytic approaches decouple the problem into two sub-problems: (1) reduce the complexity of full-body dynamics via simplified models such as the inverted pendulum [1]–[4] or the centroidal model [5]–[7] to generate high-level walking patterns, and then (2) compute feedback joint torque commands at every control loop so that the robot tracks the behavior of the simplified models. In our recent studies [8], [9], we achieved unsupported passive ankle dynamic locomotion via two computational elements: (1) a high-level footstep planner, called the Time-to-Velocity-Reversal (TVR) planner, based on the Linear Inverted Pendulum

Model (LIPM) and (2) a low-level Whole Body Controller (WBC) that tracks the desired trajectories. Although abstractions based on simplified models enable a Walking Pattern Generator (WPG) to compute footsteps efficiently in real time, they have a limited ability to represent complicated full-body motions and causes significant footstep tracking errors when the feedback controller attempts to track the desired trajectories.

On the other hand, data-driven approaches have demonstrated the possibility of robust and agile locomotion control through Reinforcement Learning (RL). Model-free RL learns a walking policy via explicit trial and error without using the knowledge of the dynamics of the robots. In [10], [11], locomotors were trained for various environments and achieved robust locomotion behaviors. In contrast, model-based RL learns a model of a robot through interactions with the environment and leverages the constructed model for planning. The approach in [12] iteratively fitted a local model for a planar walker and performed trajectory optimization, which demonstrated the ability to learn a walking policy efficiently.

Hybrid approaches have been proposed to mitigate sample inefficiency in model-free RL and improve performance in model-based RL. The work in [13] used a medium-sized neural network to approximate a robot model and initialized a model-free policy learner, which improved both data efficiency and performance for locomotion tasks. In [14], actual data originating from the environment was used to approximate dynamics, and a model-free learner optimized a policy with virtual rollouts. Instead of learning the dynamic models without prior knowledge, the work in [15], [16] learned residuals of an analytic model, whereas [17] trained control parameters to compensate for an unknown part of the dynamics.

RL with safety guarantees has been widely investigated in an effort to ensure safe exploration in the learning process and enable state-of-the-art algorithms to be deployed in real-world applications [18]. The work in [19] utilized the Hamilton-Jacobi reachability method to specify unsafe regions and switched to a safety controller when prompted. [20] proposed a more practical constrained optimization method that projects unsafe actions from a policy network to the closest and safe action. The framework in [16] generalized the constrained optimization method described above with a control barrier function and investigated strategies for action space exploration tailored to robotics. Projection-based safe learning algorithms require guidance in an action space so that the explorations made by a policy are mean-

¹J. Ahn and J. Lee are with the Department of Mechanical Engineering, the University of Texas at Austin, Austin, TX, 78712, USA {junhyeokahn91, jmlee87}@utexas.edu

^{2†}L. Sentis is with the Department of Aerospace Engineering and Engineering Mechanics, the University of Texas at Austin, Austin, TX, 78712, USA lsentis@austin.utexas.edu. He is the corresponding author.

ingful. They also need safe regions defined in advance.

In this paper, we devise a Markov Decision Process (MDP) for locomotion tasks that combining the analytic and the data-driven approaches. In contrast to other data-driven approaches in [10]–[14], [21]–[23], whose MDP takes sensor measurements and learn joint torque commands, our method solves an MDP to make a high-level decision on the desired footstep locations. It then uses a low-level WBC to evaluate locomotion behaviors and generate reward signals. Our method learns the residual dynamics of the LIPM and trains a policy for footstep location at the same time. During training, we project the footstep location onto safe regions considering the capturability metric of the LIPM and provide learning guidance using the TVR planner. More precisely, each action is designed based on three components: the TVR planner, a parameterized neural network, and a safety controller. The TVR planner computes a proper initial learning guide, which facilitates efficient learning. The parameterized neural network is trained in such a way that the long-term reward is maximized, and the safety controller guarantees safe exploration.

The proposed MDP formulation and the learning framework have the following advantages: (1) The learned policy for footstep landing locations compensates for inaccurate tracking errors. For example, the policy compensates for the effects of limb dynamics and angular momentum which cannot be represented using the LIPM; (2) our method provides data efficiency and safe exploration during the learning process; (3) we demonstrate that our framework can be used in different kind of robots for various types of locomotion.

The remainder of this paper is organized as follows. Section II describes a model-based approach for biped locomotion and DRL with safety guarantees. Section III proposes an MDP formulation and Section IV shows how we compose and update the policy to solve the proposed MDP effectively and safely. Section V evaluates the proposed framework in simulation for forward walking on a 10 Degree-of-Freedom (DoF) biped, called DRACO, and includes a turning behavior of the 23 DoF humanoid robot, ATLAS. Section VI concludes the paper.

II. PRELIMINARIES

A. Notation

\mathbb{R} and \mathbb{N} are used for the real and natural numbers, respectively. Given $a \in \mathbb{R}$ and $b \in \mathbb{R}$, where $a < b$, the set of natural numbers in the interval $[a, b]$ is expressed as $[a, b]_{\mathbb{N}}$. Given $\mathbf{x} \in \mathbb{R}^{n_x}$ and $\mathbf{y} \in \mathbb{R}^{n_y}$, $(\mathbf{x}, \mathbf{y}) := [\mathbf{x}^\top, \mathbf{y}^\top]^\top \in \mathbb{R}^{n_x+n_y}$ represents their concatenation. The $n \times m$ dimensional matrix whose elements are all one is represented by $\mathbf{1}_{n \times m}$, and the $n \times n$ identity matrix is represented as $\mathbf{I}_{n \times n}$. General Euclidean norm is denoted as $\|\mathbf{x}\| := \sqrt{\mathbf{x}^\top \mathbf{x}}$. Inner product in a vector space \mathbf{V} is represented by $\langle \cdot, \cdot \rangle : \mathbf{V} \times \mathbf{V} \mapsto \mathbb{R}$. $\mathbb{E}[\cdot]$ represents the probabilistic expectation operator.

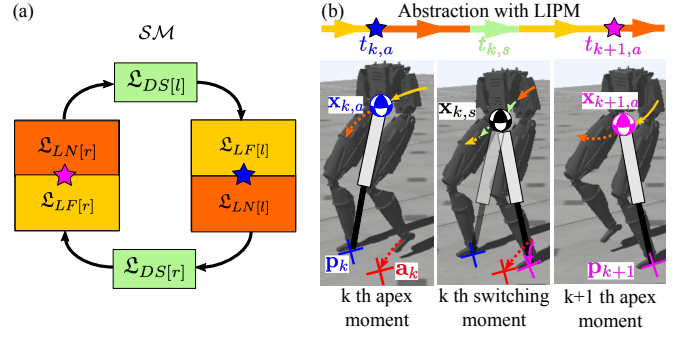


Fig. 1. (a) shows the SM for locomotion behaviors. The blue and pink stars represent the k th and $k+1$ th Apex Moments. (b) shows the walking motion with the SM and its abstraction using the LIPM.

B. An Analytic Approach to Locomotion

We define a *Locomotion State* and a state machine with simple structures to represent general locomotion behaviors.

Definition 1. (Locomotion State) A locomotion state is defined as a tuple, $\mathcal{L} := (\mathcal{L}, T_{\mathcal{L}})$.

- \mathcal{L} represents a semantic expression of locomotion behaviors: $\mathcal{L} \in \{\mathcal{L}_{DS[r/l]}, \mathcal{L}_{LF[r/l]}, \mathcal{L}_{LN[r/l]}\}$.
- The subscripts $(\cdot)_{DS[r/l]}$, $(\cdot)_{LF[r/l]}$, and $(\cdot)_{LN[r/l]}$ describe locomotion states for double support, lifting the right/left leg, and landing the right/left leg, respectively.
- $T_{\mathcal{L}}$ is a time duration for \mathcal{L} and can be chosen based on the desired stepping frequency.

Definition 2. (State Machine) We define a state machine as a sequence of Locomotion States:

$$SM := \{\mathcal{L}_{DS[r/l]}, \mathcal{L}_{LF[r/l]}, \mathcal{L}_{LN[r/l]}\}$$

- The list above is sequential in the order shown.
- The Locomotion State $\mathcal{L}_{LN[r/l]}$ terminates when a contact is detected between the swing foot and the ground.

Definition 3. (Apex Moment and Switching Moment) Given the SM defined above, an Apex Moment defines the switch between $\mathcal{L}_{LF[r/l]}$ and $\mathcal{L}_{LN[r/l]}$, and we label it as t_a . A Switching Moment defines the middle of $\mathcal{L}_{DS[r/l]}$, and we label it as t_s .

Let us consider the LIPM for our simplified model. We define the *LIPM state* as the position and velocity of the Center of Mass (CoM) of the robot on a constant height surface with an expression, $\mathbf{x} = [x, y, \dot{x}, \dot{y}]^\top \in \mathbb{R}^4$. The *LIPM stance* is defined as the location of the pivot and represented by $\mathbf{p} = [p_x, p_y]^\top \in \mathbb{R}^2$. We define the *LIPM input* as the desired location of the next stance with an expression $\mathbf{a} = [a_x, a_y]^\top \in \mathbb{R}^2$. We use the subscript k to represent properties in the k th step, for example, $\mathbf{x}_k = [x_k, y_k, \dot{x}_k, \dot{y}_k]^\top$, $\mathbf{p}_k = [p_{k,x}, p_{k,y}]^\top$, and $\mathbf{a}_k = [a_{k,x}, a_{k,y}]^\top$. We further use the subscripts k, a , and k, s to denote the properties of the robot at the Apex Moment and the Switching Moment at the k th step. For example, $\mathbf{x}_{k,a} = [x_{k,a}, y_{k,a}, \dot{x}_{k,a}, \dot{y}_{k,a}]^\top = \mathbf{x}_k(t_{k,a})$ and $\mathbf{x}_{k,s} = [x_{k,s}, y_{k,s}, \dot{x}_{k,s}, \dot{y}_{k,s}]^\top = \mathbf{x}_k(t_{k,s})$ represent the *LIPM state* evaluated at the Apex Moment and Switching Moment at the k th step, respectively. Because the

LIPM stance and *LIPM input* are invariant during the step, $\mathbf{p}_{k,a}$ and $\mathbf{a}_{k,a}$ are interchangeable with \mathbf{p}_k and \mathbf{a}_k . We also use these subscripts to describe the properties of a robot. For instance, $\phi_{k,a}^{\text{bs}} \in SO(3)$ and $\mathbf{w}_{k,a}^{\text{bs}} \in \mathbb{R}^3$ represent the orientation and angular velocity of a base link, respectively, and $\phi_{k,a}^{\text{pv}} \in SO(3)$ represents the orientation of a stance foot (a pivot) with respect to the world frame at the *Apex Moment* at the k th step. Fig. 1 illustrates the *SM* and the abstraction of the locomotion behavior with the LIPM.

The goal of the WPG is to generate \mathbf{a}_k and the CoM trajectory based on $\mathbf{x}_{k,a}$ and \mathbf{p}_k at the *Apex Moment*. From the walking pattern, the low-level WBC provides the computation of sensor-based feedback control loops and torque command for the robot to track the desired location of the next stance and the CoM trajectory. Note that the WPG designs the pattern at the *Apex Moment* at each step, while the WBC computes the feedback torque command at every control loop.

C. TVR Planner

The differential equation of the LIPM is represented as follows:

$$\dot{\mathbf{x}}(t) = \begin{bmatrix} 0 & 0 & 1 & 0 \\ 0 & 0 & 0 & 1 \\ g/h & 0 & 0 & 0 \\ 0 & g/h & 0 & 0 \end{bmatrix} \mathbf{x}(t) - \begin{bmatrix} 0 & 0 \\ g/h & 0 \\ 0 & g/h \end{bmatrix} \mathbf{p}, \quad (1)$$

where g is the gravitational constant and h is the constant height of the CoM of the point mass.

At the k th step, given an initial condition $\mathbf{x}_k(0) = \mathbf{x}_{k,0}$ and a stance position \mathbf{p}_k , the solution of Eq. (1) yields a state transition map Ψ , with the expression

$$\mathbf{x}_k(t) = \Psi(t; \mathbf{x}_{k,0}, \mathbf{p}_k) = f_\Psi(t)\mathbf{x}_{k,0} + g_\Psi(t)\mathbf{p}_k, \quad (2)$$

where

$$f_\Psi(t) := \begin{bmatrix} C_1(t) & 0 & C_2(t) & 0 \\ 0 & C_1(t) & 0 & C_2(t) \\ C_3(t) & 0 & C_1(t) & 0 \\ 0 & C_3(t) & 0 & C_1(t) \end{bmatrix},$$

$$g_\Psi(t) := \begin{bmatrix} 1 - C_1(t) & 0 \\ 0 & 1 - C_1(t) \\ -C_3(t) & 0 \\ 0 & -C_3(t) \end{bmatrix},$$

$C_1(t) := \cosh(\omega t)$, $C_2(t) := \sinh(\omega t)/\omega$, and $C_3(t) := \omega \sinh(\omega t)$, and $\omega := \sqrt{g/h}$, respectively.

Because the TVR planner determines the desired location of the next stance at the *Apex Moment* (i.e., $t = t_{k,a}$), we set the initial condition as $\mathbf{x}_k(0) = \mathbf{x}_{k,a}$. With pre-specified time duration $T_{\mathcal{L}_{LN}[r/l]}$, we compute the state at the *Switching Moment* as

$$\mathbf{x}_{k,s} = \mathbf{x}_k(T_{\mathcal{L}_{LN}[r/l]}) = \Psi(T_{\mathcal{L}_{LN}[r/l]}; \mathbf{x}_k(t_{k,a}), \mathbf{p}_k). \quad (3)$$

From $\mathbf{x}_{k,s}$, the TVR planner computes \mathbf{a}_k , such that the sagittal velocity \dot{x} (and lateral velocity \dot{y} , respectively) of the CoM is driven to zero at the predefined time intervals

$T_{x'}$ (and $T_{y'}$, respectively) after the LIPM switches to the new stance. These constraints are expressed as

$$0 = \langle \boldsymbol{\xi}_j, \Psi(T_j; \mathbf{x}_{k,s}, \mathbf{a}_k) \rangle, \quad j \in \{x', y'\}, \quad (4)$$

where $\boldsymbol{\xi}_{x'} := [0, 0, 1, 0]^\top$ and $\boldsymbol{\xi}_{y'} := [0, 0, 0, 1]^\top$. From Eq. (4), \mathbf{a}_k is computed with an additional bias term κ_x and κ_y as

$$\mathbf{a}_k^{\text{TVR}} = \Phi(\mathbf{x}_{k,s}) = f_\Phi(T_{x'}, T_{y'})\mathbf{x}_{k,s} + g_\Phi, \quad (5)$$

where

$$f_\Phi(T_{x'}, T_{y'}) := \begin{bmatrix} 1 - \kappa_x & 0 & C_4(T_{x'}) & 0 \\ 0 & 1 - \kappa_y & 0 & C_4(T_{y'}) \end{bmatrix},$$

$$g_\Phi := \begin{bmatrix} \kappa_x & 0 \\ 0 & \kappa_y \end{bmatrix} \begin{bmatrix} x^d \\ y^d \end{bmatrix},$$

$C_4(T) := \frac{e^{\omega T} + e^{-\omega T}}{w(e^{\omega T} - e^{-\omega T})}$ and $[x^d, y^d]^\top \in \mathbb{R}^2$ represents a desired position for the CoM of the robot. Note that Eq. (5) is a simple proportional-derivative controller and that $T_{x'}$, $T_{y'}$, κ_x , and κ_y are the gain parameters used to keep the CoM converging to the desired position. A more detailed derivation of the LIPM was described in [24].

D. Reinforcement Learning with Safety Guarantees

Consider an infinite-horizon discounted MDP with control-affine, deterministic dynamics defined by the tuple $(\mathcal{S}, \mathcal{A}, \mathcal{T}, r, \rho_0, \gamma)$, where \mathcal{S} is a set of states, \mathcal{A} is a set of actions, $\mathcal{T} : \mathcal{S} \mapsto \mathcal{S}$ is the deterministic dynamics, in our case affine in the controls, $r : \mathcal{S} \times \mathcal{A} \mapsto \mathbb{R}$ is the reward function, $\rho_0 : \mathcal{S} \mapsto \mathbb{R}$ is the distribution of the initial state, and $\gamma \in (0, 1)$ is the discount factor. The control affine dynamics are written as

$$\mathbf{s}_{k+1} = f(\mathbf{s}_k) + g(\mathbf{s}_k)\mathbf{a}_k + d(\mathbf{s}_k), \quad (6)$$

where $\mathbf{s}_k \in \mathcal{S} \subseteq \mathbb{R}^{n_s}$, and $\mathbf{a}_k \in \mathcal{A} \subset \mathbb{R}^{n_a}$ represent a state and input, respectively. $f : \mathcal{S} \mapsto \mathcal{S}$, and $g : \mathcal{S} \mapsto \mathbb{R}^{n_s \times n_a}$ are the analytic underactuated and actuated dynamics, respectively, while $d : \mathcal{S} \mapsto \mathcal{S}$ is the unknown part of the system dynamics. Moreover, let $\pi_\theta(\mathbf{a}|\mathbf{s})$ represent a stochastic control policy parameterized by a vector θ . $\pi_\theta : \mathcal{S} \times \mathcal{A} \mapsto \mathbb{R}_{\geq 0}$ maps states to distributions over actions, and $V_{\pi_\theta}(\mathbf{s})$ represents the policy's expected discounted reward with the expression

$$V_{\pi_\theta}(\mathbf{s}_k) = \mathbb{E}_{\tau \sim \pi_\theta} \left[\sum_{i=0}^{\infty} \gamma^i r(\mathbf{s}_{k+i}, \mathbf{a}_{k+i}) \right], \quad (7)$$

where $\tau \sim \pi_\theta$ is a trajectory drawn from the policy π_θ (e.g., $\tau = [\mathbf{s}_k, \mathbf{a}_k, \dots, \mathbf{s}_{k+n}, \mathbf{a}_{k+n}]$).

For safe exploration in the learning process under uncertain dynamics, [16], [19] employed a Gaussian Process (GP) to approximate the unknown part of the dynamics from the dataset by learning a mean estimate $\boldsymbol{\mu}_d(\mathbf{s})$ and an uncertainty $\boldsymbol{\sigma}_d^2(\mathbf{s})$ in tandem with the policy update with probability confidence intervals on the estimation,

$$\boldsymbol{\mu}_d(\mathbf{s}) - k_\delta \boldsymbol{\sigma}_d(\mathbf{s}) \leq d(\mathbf{s}) \leq \boldsymbol{\mu}_d(\mathbf{s}) + k_\delta \boldsymbol{\sigma}_d(\mathbf{s}), \quad (8)$$

where k_δ is a design parameter for confidence (e.g., $k_\delta = 2$ for 95% confidence). Then, the control input is computed to keep the following state within a given invariant safe set $\mathcal{C} = \{\mathbf{s} \in \mathcal{S} \mid h(\mathbf{s}) \geq 0\}$ by computing

$$\sup_{\mathbf{a}_k \in \mathcal{A}} [h(f(\mathbf{s}_k) + g(\mathbf{s}_k)\mathbf{a}_k + d(\mathbf{s}_k)) + (\eta - 1)h(\mathbf{s}_k)] \geq 0, \quad (9)$$

where $\eta \in [0, 1]$.

III. MDP FORMULATION

We define a set of states \mathcal{S} and a set of actions \mathcal{A} associated with the *Apex Moment* at each step:

$$\begin{aligned} \mathcal{S} &:= \{(\mathbf{x}_{k,a}, \mathbf{p}_{k,a}, \phi_{k,a}^{\text{bs}}, \mathbf{w}_{k,a}^{\text{bs}}, \phi_{k,a}^{\text{pv}}) \mid \forall k \in [1, m]_{\mathbb{N}}\}, \\ \mathcal{A} &:= \{\mathbf{a}_{k,a} \mid \forall k \in [1, m]_{\mathbb{N}}\}, \end{aligned}$$

where m can be set as $+\infty$ when considering the infinite steps of the locomotion.

Recall from the nomenclatures in Section II-B that $\mathbf{x}_{k,a}$, $\mathbf{p}_{k,a}$ and $\mathbf{a}_{k,a}$ are the expressions of the *LIPM state*, *LIPM stance*, and *LIPM input* evaluated at the *Apex Moment*. Note that $\mathbf{p}_{k,a}$ and $\mathbf{a}_{k,a}$ are interchangeable with \mathbf{p}_k and \mathbf{a}_k . Moreover, $\phi_{k,a}^{\text{bs}}$ and $\mathbf{w}_{k,a}^{\text{bs}}$ represent the orientation and angular velocity of a base link and $\phi_{k,a}^{\text{pv}}$ expresses an orientation of the stance foot at the *Apex Moment*.

We divide the state into two parts as

$$\begin{aligned} \mathbf{s}_{k+1} &= [\mathbf{s}_{k+1}^u \mid \mathbf{s}_{k+1}^l]^\top \\ &= [\mathbf{x}_{k+1,a} \quad \mathbf{p}_{k+1} \mid \phi_{k+1,a}^{\text{bs}} \quad \mathbf{w}_{k+1,a}^{\text{bs}} \quad \phi_{k+1,a}^{\text{pv}}]^\top \end{aligned}$$

and define a transition function for the upper part of the state based on Eq. (2) as

$$\begin{aligned} \mathbf{s}_{k+1}^u &= f(\mathbf{x}_{k,a}, \mathbf{p}_k) + g\mathbf{a}_k + d(\mathbf{x}_{k,a}, \mathbf{p}_k), \\ f(\mathbf{x}_{k,a}, \mathbf{p}_k) &:= \begin{bmatrix} f_\Psi(T_{LF})\Psi(T_{LN}; \mathbf{x}_{k,a}, \mathbf{p}_k) \\ \mathbf{0}_{2 \times 1} \end{bmatrix}, \quad (10) \\ g &:= \begin{bmatrix} g_\Psi(T_{LF}) \\ \mathbf{I}_{2 \times 2} \end{bmatrix}. \end{aligned}$$

$d(\mathbf{x}_{k,a}, \mathbf{p}_k)$ represents the unknown part of the dynamics fitted via Eq. (8)¹. The uncertainties are attributed to the discrepancies between the simplified model and the actual robot. Note that the dynamics of the lower part of the states, \mathbf{s}_{k+1}^l , cannot be expressed in closed form. Therefore, we optimize our policy in a model-free sense, but utilize the LIPM to provide safe exploration and data efficiency in the learning process.

To improve the locomotion behavior, we define the following reward function:

$$r(\mathbf{s}_k, \mathbf{a}_k) = r_a + r_b(\mathbf{s}_k) + r_t(\mathbf{s}_k) + r_s(\mathbf{s}_k) + r_c(\mathbf{a}_k). \quad (11)$$

Given $\mathbf{w}_{k,a}^{\text{bs}} = [w_{k,x}, w_{k,y}, w_{k,z}]^\top$, the Euler ZYX representation $[\phi_{k,x}^{\text{bs}}, \phi_{k,y}^{\text{bs}}, \phi_{k,z}^{\text{bs}}]^\top$ of ϕ_k^{bs} and $[\phi_{k,x}^{\text{pv}}, \phi_{k,y}^{\text{pv}}, \phi_{k,z}^{\text{pv}}]^\top$ of ϕ_k^{pv} , r_a is an alive bonus, $r_b(\mathbf{s}_k) := -w_b \|(\phi_{k,x}^{\text{bs}}, \phi_{k,y}^{\text{bs}})\|^2$ penalizes the roll and pitch variation to keep the body upright, $r_t(\mathbf{s}_k) := -w_t \|(\dot{x}_{k,a}^d, \dot{y}_{k,a}^d, \phi_{k,z}^{\text{bs,d}}, \phi_{k,z}^{\text{pv,d}}) -$

$(x_k, y_k, \phi_{k,z}^{\text{bs}}, \phi_{k,z}^{\text{pv}})\|^2$ penalizes divergence from the desired CoM positions and the heading of the robot, $r_s(\mathbf{s}_k) := -w_s \|(\dot{x}_{k,a}^d, \dot{y}_{k,a}^d, w_{k,z}^d) - (\dot{x}_{k,a}, \dot{y}_{k,a}, w_{k,z})\|^2$ is for steering the robot with a desired velocity, and $r_c(\mathbf{a}_k) := -w_c \|\mathbf{a}_k\|^2$ penalizes excessive control input.

IV. POLICY DESIGN AND UPDATE

Our goal is to learn an optimal policy for desired foot locations. We use the Proximal Policy Optimization (PPO) [21] to learn the policy iteratively. PPO defines an advantage function $A_{\pi_\theta}(\mathbf{s}_k, \mathbf{a}_k) := Q_{\pi_\theta}(\mathbf{s}_k, \mathbf{a}_k) - V_{\pi_\theta}(\mathbf{s}_k)$, where $Q_{\pi_\theta}(\mathbf{s}_k, \mathbf{a}_k)$ is the state-action value function that evaluates the return of taking action \mathbf{a}_k at state \mathbf{s}_k and following the policy π thereafter. By maximizing a modified objective function

$$L_{\text{PPO}}(\boldsymbol{\theta}) = \mathbb{E}_{\tau \sim \pi_\theta} [\min(r_k A_k, \text{clip}(r_k, 1 - \epsilon, 1 + \epsilon) A_k)],$$

where $r_k := \frac{\pi_\theta(\mathbf{a}_k | \mathbf{s}_k)}{\pi_{\theta_{\text{old}}}(\mathbf{a}_k | \mathbf{s}_k)}$ is the importance resampling term that allows us to use the dataset under the old policy $\pi_{\theta_{\text{old}}}$ to estimate for the current policy π_θ . A_k is a short notation for $A_{\pi_\theta}(\mathbf{s}_k, \mathbf{a}_k)$. The max and *clip* operator ensures that the policy π_θ does not change excessively from the old policy $\pi_{\theta_{\text{old}}}$.

A. Safe Set Approximation

The work in [25] introduced an instantaneous capture point that enables the LIPM to come to a stop if it places and maintains its stance there instantaneously. Here, we consider i -step capture regions for the LIPM at the *Apex Moment*:

$$\left\| \begin{bmatrix} 1 & 0 & 1/\omega & 0 & -1 & 0 \\ 0 & 1 & 0 & 1/\omega & 0 & -1 \end{bmatrix} \begin{bmatrix} \mathbf{x}_{k,a} \\ \mathbf{p}_k \end{bmatrix} \right\| \leq \mathcal{CP}_i, \quad (12)$$

where

$$\begin{aligned} \mathcal{CP}_1 &:= l_{\max} e^{-T_{\mathcal{L}LN[r/i]}}, \\ \mathcal{CP}_2 &:= l_{\max} e^{-T_{\mathcal{L}LN[r/i]}} (1 + e^{-T_{\mathcal{L}LN[r/i]}}), \end{aligned}$$

$\omega = \sqrt{g/h}$, and l_{\max} is the maximum step length that the LIPM can reach. Both ω and l_{\max} are achieved from the kinematics of a robot. $T_{\mathcal{L}LN[r/i]}$ is a predefined temporal parameter that represents the time period until the robot lands its swing foot. We conservatively approximate the ellipsoid of Eq. (12) with a polytope and define the safe set as

$$\mathcal{C} = \{(\mathbf{x}_{k,a}, \mathbf{p}_k) \mid h(\mathbf{x}_{k,a}, \mathbf{p}_k) \geq \mathbf{0}_{4 \times 1}, \forall k \in [1, m]_{\mathbb{N}}\}, \quad (13)$$

where

$$\begin{aligned} h(\mathbf{x}_{k,a}, \mathbf{p}_k) &:= \mathbf{A}_C \begin{bmatrix} \mathbf{x}_{k,a} \\ \mathbf{p}_k \end{bmatrix} + \mathbf{b}_C, \\ \mathbf{A}_C &:= \frac{1}{\mathcal{CP}_i} \begin{bmatrix} -1 & -1 & -1/\omega & -1/\omega & 1 & 1 \\ -1 & 1 & -1/\omega & 1/\omega & 1 & -1 \\ 1 & -1 & 1/\omega & -1/\omega & -1 & 1 \\ 1 & 1 & 1/\omega & 1/\omega & -1 & -1 \end{bmatrix}, \quad (14) \\ \mathbf{b}_C &:= \mathbf{1}_{4 \times 1}. \end{aligned}$$

The safe set in Eq. (13) represents the set of the *LIPM state* and *LIPM stance* pairs that could be stabilized without falling

¹We use a squared exponential kernel for GP prior to implementation.

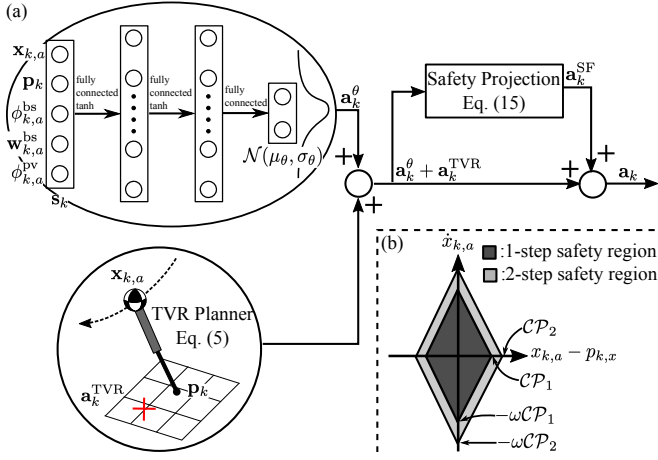


Fig. 2. (a) The design of the safety-guaranteeing policy, \mathbf{a}_k . (b) The projection onto the x and \dot{x} plane of the one- and two-step capture regions of the LIPM.

by taking i -step. In other words, if an *LIPM state* and *LIPM stance* pair is inside the safe set at the k th step, there is always a location for the next stance \mathbf{a}_k (and the following stance \mathbf{a}_{k+1} in the case of two-step capture region) that stabilizes the LIPM. The projection onto the x and \dot{x} plane of capture regions is represented in Fig. 2(b).

B. Safety Guaranteeing Policy Design

For data-efficient and safe learning, we design our control input with three components:

$$\mathbf{a}_k = \mathbf{a}_k^{\text{TVR}} + \mathbf{a}_k^\theta + \mathbf{a}_k^{\text{SF}}(\mathbf{a}_k^{\text{TVR}} + \mathbf{a}_k^\theta), \quad (15)$$

where $\mathbf{a}_k^{\text{TVR}} = \Phi(\Psi(T_{LN}, 0; \mathbf{x}_k, \mathbf{p}_k))$ is computed by the TVR planner and \mathbf{a}_k^θ is drawn from a parameterized Gaussian distribution, $\mathcal{N}(\boldsymbol{\mu}_\theta, \boldsymbol{\sigma}_\theta)$, where $\boldsymbol{\mu}_\theta$ and $\boldsymbol{\sigma}_\theta$ denote a mean vector and covariance matrix parameterized by $\boldsymbol{\theta}^2$, respectively.

Given arbitrary $\mathbf{a}_k^{\text{TVR}}$ and \mathbf{a}_k^θ , the safety-guaranteeing controller \mathbf{a}_k^{SF} ensures the following *LIPM state* and *LIPM stance* pair $(\mathbf{x}_{k+1,a}, \mathbf{p}_{k+1})$ steered by the final control input (\mathbf{a}_k) stays inside the safe set \mathcal{C} . In our problem, Eq. (9) is modified as

$$\sup_{\mathbf{a}_k^{\text{SF}}} [h(\mathbf{x}_{k+1,a}, \mathbf{p}_{k+1}) + (\eta - 1)h(\mathbf{x}_{k,a}, \mathbf{p}_k)] \geq \mathbf{0}_{4 \times 1}. \quad (16)$$

Substituting Eq. (10) and Eq. (14) into Eq. (16), and choosing the worst case for the uncertain dynamics in Eq. (8) yields the following inequality constraint:

$$\begin{aligned} & \mathbf{A}_C \left(f(\mathbf{x}_{k,a}, \mathbf{p}_k) + g(\mathbf{a}_k^{\text{TVR}} + \mathbf{a}_k^\theta + \mathbf{a}_k^{\text{SF}}) + \boldsymbol{\mu}_d(\mathbf{x}_{k,a}, \mathbf{p}_k) \right. \\ & \left. - |k_\delta \boldsymbol{\sigma}_d(\mathbf{x}_{k,a}, \mathbf{p}_k)| \right) + \mathbf{b}_C \geq (1 - \eta) \left(\mathbf{A}_C \begin{bmatrix} \mathbf{x}_{k,a} \\ \mathbf{p}_k \end{bmatrix} + \mathbf{b}_C \right). \end{aligned} \quad (17)$$

Considering the safety constraint in Eq. (17) and input boundaries, the optimization problem is summarized in

²In the implementation, we choose two fully connected hidden layers with the tanh activation function.

Algorithm 1: Policy Learning Process

Data: Number of episode M , Number of data samples K

Result: π_θ

Initialize $\pi_\theta, \mathbf{s}_0 \sim \rho_0$, data array D ;

for $m = 1 : M$ **do**

for $k = 1 : K$ **do**

$\mathbf{a}_k^\theta \sim \pi_\theta, \mathbf{a}_k^{\text{TVR}} \leftarrow \text{Eq. (5)} ;$

$\mathbf{a}_k^{\text{SF}} \leftarrow \text{Eq. (18)} ;$

$\mathbf{a}_k \leftarrow \text{Eq. (15)} ;$

$r_k \leftarrow \text{Eq. (11)} ;$

$\mathbf{s}_{k+1,a} \leftarrow \text{WBC stabilizes the robot and brings it to the next Apex Moment} ;$

store $(\mathbf{s}_k, \mathbf{a}_k, \mathbf{s}_{k+1}, r_k)$ in D ;

end

$\pi_\theta \leftarrow \text{Optimize } L_{\text{PPO}} \text{ with } D \text{ w.r.t } \boldsymbol{\theta} ;$

Update GP model with D ;

clear D ;

end

the following Quadratic Programming (QP) and efficiently solved for the safety compensation as

$$\begin{aligned} \min_{\mathbf{a}_k^{\text{SF}}, \epsilon} & \quad \|\mathbf{a}_k^{\text{SF}}\| + K_\epsilon \epsilon \\ \text{s.t.} & \quad \begin{bmatrix} \mathbf{A}_{\text{qp}}^{(11)} & \mathbf{A}_{\text{qp}}^{(12)} \\ \mathbf{A}_{\text{qp}}^{(21)} & \mathbf{A}_{\text{qp}}^{(22)} \\ \mathbf{A}_{\text{qp}}^{(31)} & \mathbf{A}_{\text{qp}}^{(32)} \end{bmatrix} \begin{bmatrix} \mathbf{a}_k^{\text{SF}} \\ \epsilon \end{bmatrix} \leq \begin{bmatrix} \mathbf{b}_{\text{qp}}^{(1)} \\ \mathbf{b}_{\text{qp}}^{(2)} \\ \mathbf{b}_{\text{qp}}^{(3)} \end{bmatrix}, \end{aligned} \quad (18)$$

where ϵ is a slack variable in the safety constraint, and K_ϵ is a large constant to penalize safety violation. Here,

$$\begin{aligned} \mathbf{A}_{\text{qp}}^{(11)} &= -\mathbf{A}_C g, & \mathbf{A}_{\text{qp}}^{(12)} &= -\mathbf{1}_{4 \times 1}, & \mathbf{A}_{\text{qp}}^{(21)} &= \mathbf{I}_{2 \times 2}, \\ \mathbf{A}_{\text{qp}}^{(22)} &= \mathbf{0}_{2 \times 1}, & \mathbf{A}_{\text{qp}}^{(31)} &= -\mathbf{I}_{2 \times 2}, & \mathbf{A}_{\text{qp}}^{(32)} &= \mathbf{0}_{2 \times 1}, \end{aligned}$$

and

$$\begin{aligned} \mathbf{b}_{\text{qp}}^{(1)} &= \mathbf{A}_C (f(\mathbf{x}_{k,a}, \mathbf{p}_k) + \boldsymbol{\mu}_d(\mathbf{x}_{k,a}, \mathbf{p}_k) + g(\mathbf{a}_k^{\text{TVR}} + \mathbf{a}_k^\theta) \\ & \quad - (1 - \eta) \mathbf{A}_C \begin{bmatrix} \mathbf{x}_{k,a} \\ \mathbf{p}_k \end{bmatrix} - k_\delta |\mathbf{A}_C \boldsymbol{\sigma}_d(\mathbf{x}_{k,a}, \mathbf{p}_k)| + \eta \mathbf{b}_C), \end{aligned}$$

$$\begin{aligned} \mathbf{b}_{\text{qp}}^{(2)} &= -(\mathbf{a}_k^{\text{TVR}} + \mathbf{a}_k^\theta) + \mathbf{a}_{\text{max}} \\ \mathbf{b}_{\text{qp}}^{(3)} &= (\mathbf{a}_k^{\text{TVR}} + \mathbf{a}_k^\theta) - \mathbf{a}_{\text{min}}. \end{aligned}$$

The first segment of the inequality represents a constraint for the safety, and the last two are for the input constraints. The design of the safety-guaranteeing policy is illustrated in Fig. 2(a). Based on the MDP formulation and the policy design, the overall algorithm for efficient and safe learning for locomotion behaviors is summarized in Alg. 1.

C. Further Details

It is worth taking a look at each of the components in the final action described by Eq. (15). $\mathbf{a}_k^{\text{TVR}} + \mathbf{a}_k^\theta$ provides a “feedforward exploration” in the state space, where the stochastic action explores the TVR planner and optimizes the long-term reward. \mathbf{a}_k^{SF} projects $\mathbf{a}_k^{\text{TVR}} + \mathbf{a}_k^\theta$ onto the safe set of policies and furnishes “safety compensation”.

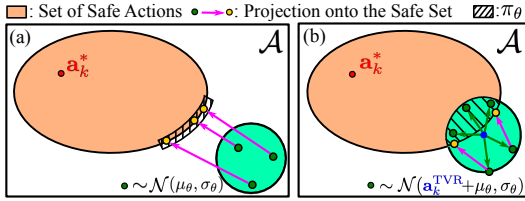


Fig. 3. The safety compensation process. \mathbf{a}_k^* denotes an optimal control input and the orange area represents a set of safe actions that ensures that the state at the next time step stays inside the safe set \mathcal{C} . (a) and (b) represent two different instances of feedforward exploration.

Particularly, $\mathbf{a}_k^{\text{TVR}}$ in the feedforward exploration provides learning guidance and resolves two major issues in the safety projection: (1) inactive exploration and (2) the credit assignment problem. Consider, for example, two cases with different feedforward explorations, as illustrated in Fig. 3, whose final control policies are: (a) $\mathbf{a}_k = \mathbf{a}_k^\theta + \mathbf{a}_k^{\text{SF}}(\mathbf{a}_k^\theta)$ and (b) $\mathbf{a}_k = \mathbf{a}_k^{\text{TVR}} + \mathbf{a}_k^\theta + \mathbf{a}_k^{\text{SF}}(\mathbf{a}_k^{\text{TVR}} + \mathbf{a}_k^\theta)$.

In the case of (a) (and (b), respectively), the cyan area represents feedforward exploration expressed by a Gaussian distribution $\mathcal{N}(\mu_\theta, \sigma_\theta)$ (and $\mathcal{N}(\mathbf{a}_k^{\text{TVR}} + \mu_\theta, \sigma_\theta)$, respectively), and the green dots are its samples. The pink arrow represents the safety compensation $\mathbf{a}_k^{\text{SF}}(\mathbf{a}_k^\theta)$ (and $\mathbf{a}_k^{\text{SF}}(\mathbf{a}_k^{\text{TVR}} + \mathbf{a}_k^\theta)$, respectively). The black striped area is a distribution of the final action \mathbf{a}_k , and the yellow dots are its sample.

As Fig. 3(a) shows, there is no intersection between the set of safe actions and the possible feedforward exploration and the feedforward explorations are all projected onto the safe action set. The projection does not preserve the volume in the action space, and it hinders active explorations in the learning. However, Fig. 3(b) leverages the TVR planner as learning guidance and retains the volume in action space to explore over. When it comes to computing a gradient of the long-term reward, the projected actions make it difficult to evaluate the resulting trajectories and assign the credits in the θ space. In other words, as Fig. 3(a) shows, three compensated samples (yellow dots) do not roll out different trajectories, which prevents the gradient descent and results in a local optimum.

V. SIMULATION RESULTS

Our proposed MDP formulation and the policy design could be applied to any humanoid to achieve versatile locomotion behavior. In this section, we evaluate our framework via a forward walking with 10-DoF DRACO biped [9] and 23-DoF Boston Dynamic’s ATLAS humanoid in DART simulator [26].

Especially, we train five different policies to demonstrate the effectiveness of our formulation. First, we train policies with (1) the method in other data-driven approaches described in Section I but use DRACO and ATLAS to achieve the desired walking behavior.³ Moreover, we solve our proposed MDP by alternating the components of the action in Eq. (15): (2) $\mathbf{a}^\theta + \mathbf{a}^{\text{TVR}}$ with a tight bound on the action, (3) $\mathbf{a}^\theta + \mathbf{a}^{\text{SF}}$, and $\mathbf{a}^\theta + \mathbf{a}^{\text{TVR}} + \mathbf{a}^{\text{SF}}$ with (4) one-step and (5) two-step safety regions. A turning behavior with ATLAS is further simulated to demonstrate that our MDP accomplishes different types of locomotion behavior. However, in the turning simulation, we do not consider to train policies using other data-driven approaches because it is challenging to achieve the desired behavior using them.

DRACO has small, lightweight feet without ankle roll actuation and a relatively small number of DoF compared to ATLAS. Therefore, the low-level WBC in the DRACO simulation only controls the position of the feet, the roll and pitch of the torso, and the height of the CoM, whereas in the ATLAS simulation, it controls the position and orientation of the feet, the orientation of torso, and the position of the CoM. We demonstrate only the turning behavior with ATLAS due to the mechanical difference and limited DOF. DRACO requires quicker stepping motion due to the small, passive feet, so we use smaller values for the temporal parameters in the \mathcal{SM} for DRACO. Parameters used in the simulations are summarized in Table I.

A. Forward Walking

Multiple policies are trained in five different setups for DRACO and ATLAS to regulate forward walking; the learning processes, as well as baseline performance of the TVR, are illustrated in Fig. 4 with some useful metrics. In DRACO and ATLAS forward walking, training policies with other data-driven approaches takes a more substantial dataset (denoted by Δ) to generate desired locomotion behavior than using the proposed MDP. Note that the method used in other data-driven approaches has a formulation different from our MDP; the average return in Fig. 4 has a different scale.

The process using the conservative one-step capture region (blue curve) helps to accelerate the learning at the beginning phase, but the one using the relaxed two-step capture region (orange curve) eventually achieves a better walking policy in

³Other data-driven approaches produce reward signals with the forward displacement and velocity of the robot. Readers are referred to Appendix B in [12] for more details about environment setups.

TABLE I
SIMULATION PARAMETERS.

	LIPM	\mathcal{SM}	\mathbf{a}^{TVR}	\mathbf{a}^θ	\mathbf{a}^{SF}	Reward					Behavior
	$[h, l_{\max}]$	$[T_{LN}, T_{LF}]$	$[T_{x'}, T_{y'}, \kappa_x, \kappa_y]$	Layer	$[K_\epsilon, \eta]$	r_a	w_b	w_t	w_s	w_c	$[\dot{x}^d, \omega_z^d]$
DRACO Walking	[0.93, 0.7]	[0.16, 0.16]	[0.22, 0.22, -0.18, -0.18]	[64, 64]	$[10^5, 0.8]$	5.0	3.0	3.0	1.0	1.0	[0.3, 0]
ATLAS Walking	[0.82, 0.55]	[0.23, 0.23]	[0.15, 0.15, -0.16, -0.16]	[64, 64]	$[10^5, 0.8]$	5.0	3.0	3.0	1.0	1.0	[0.15, 0]
ATLAS Turning	[0.82, 0.55]	[0.23, 0.23]	[0.15, 0.15, -0.16, -0.16]	[64, 64]	$[10^5, 0.8]$	5.0	5.0	5.0	3.0	1.0	[0, 0.09]

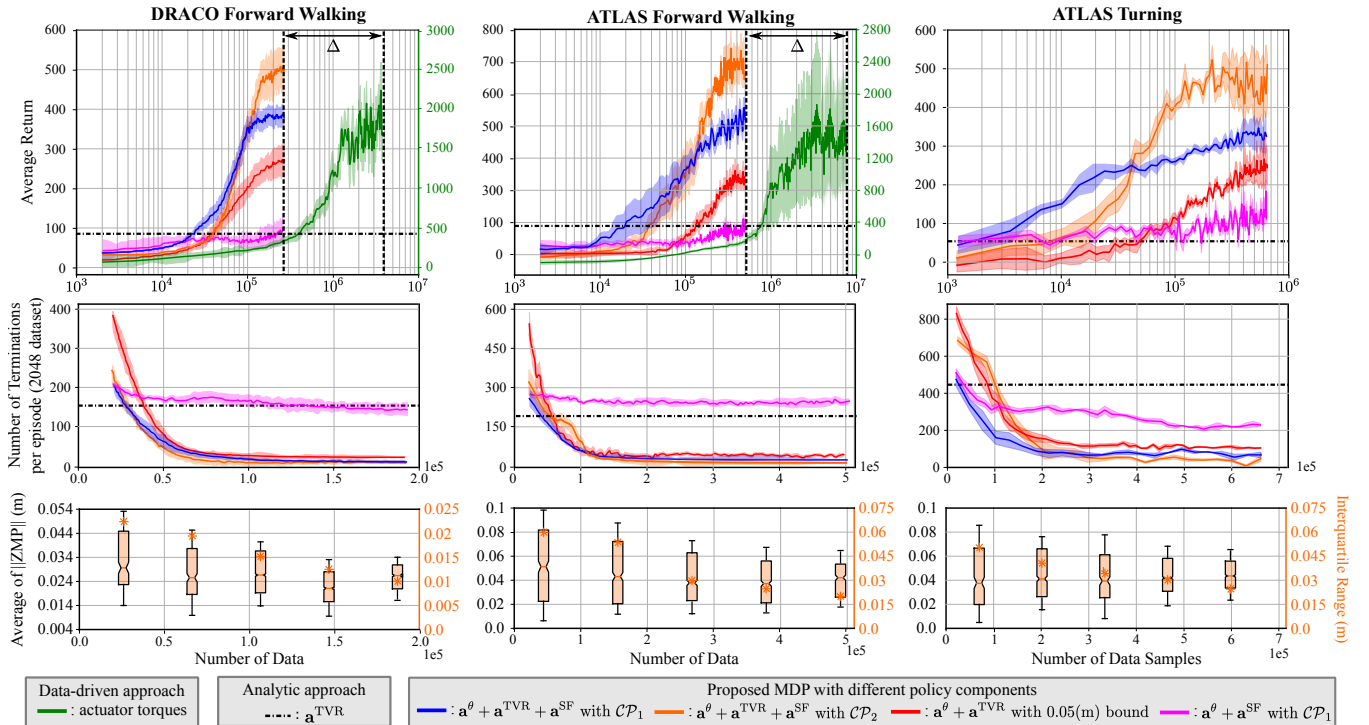


Fig. 4. Learning curves of five different setups are illustrated for forward walking and turning with the baseline performance of the TVR planner. The average return, the number of terminations per episode, and the average of two-norm of ZMP in the local frame from above are shown throughout the training. Each of the curves is plotted with the mean and standard deviation across five runs. In the average return graphs, the x -axis uses a logarithm scale. Note that the data-driven approach represented by the green curve in the average return plot should be read with the axis on the right. The orange asterisks in the ZMP plot illustrate the interquartile range of the box plot.

terms of the average return. Training without using the safety projection (red curve) exhibits relatively good performance, whereas the one without the TVR planner (pink curve) rarely improves throughout the updates. The result reflects the issues addressed in Section IV-C.

The number of terminations per episode decays as the uncertain parts of the dynamics are revealed throughout the training. We further show the average of two-norm of Zero-Moment-Points (ZMP), which has been a significant indicator for dynamic balancing as described in [27], and argue that the policy learning enhances the locomotion capability along the learning process. The decrement of the interquartile of the box plot indicates that less ankle actuation is used in locomotion, which results in less shaky locomotion.

We pick a trained policy from the process (orange curve) where the policy is composed of the TVR planner and two-step safety projection to evaluate walking behavior. In Fig. 5(a), (b), and (c), forward walking is shown along with the SM without a safety violation.

B. Turning

Multiple policies are trained for the turning behavior with various policy setups and illustrated in Fig. 4. Learning the footstep placement for turning takes a similar number of data samples as it does for walking. Observations of the learning processes shown in Fig. 4 are analogous to the ones in forward walking. Note that because the LIPM itself is not informative enough to address turning behavior, there are many more terminations at the beginning compared to

forward walking. However, as the residuals of the model are trained, and the parameterized neural network learns to adjust the landing location, the number of terminations decays. The magnitudes in the ZMP plot tend to be smaller than the ones in ATLAS forward walking, because ZMP varies more along the lateral direction than the sagittal direction in turning behavior.

We choose a policy from the setup (orange curve) where the policy is composed of the TVR planner and two-step safety projection to evaluate turning behavior. Fig. 5 (d) and (e) shows the turning behavior regulated by the SM along the time axis. Turning simulation demonstrates that other versatile locomotion behaviors could be achieved using the proposed MDP without increasing the complexity of the problem.

VI. CONCLUDING REMARKS

In this letter, we describe an MDP formulation for data-efficient and safe learning for locomotion. Our formulation combines the analytic and data-driven approaches to make a high-level footstep decision using the LIPM. In the learning process, we learn the transition function of the MDP using GP based on the LIPM so that we compensate for behaviors outside of the LIPM. We design our policy in combination with the TVR planner, the parameterized neural network, and the safety-guaranteeing controller, which enables safe and data-efficient learning. We evaluate our framework's effectiveness through simulations of walking and turning.

We plan to implement this framework into real bipedal

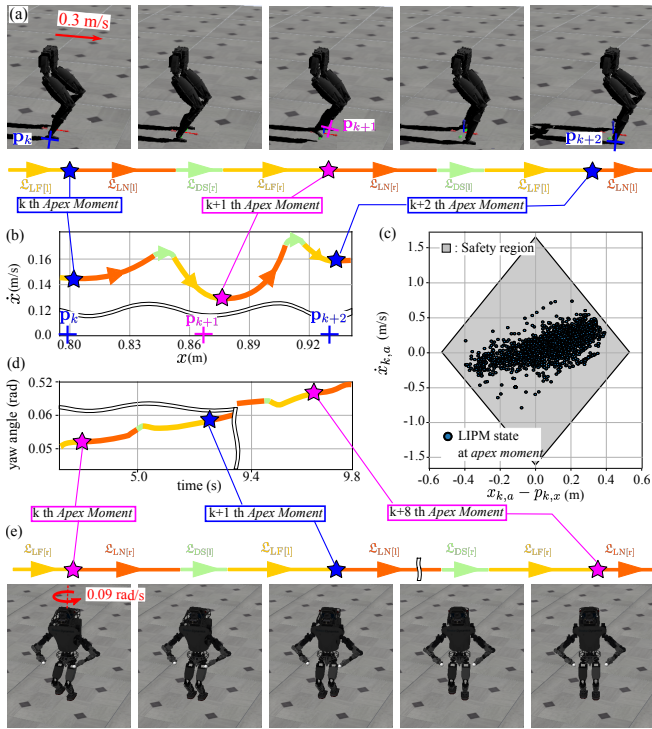


Fig. 5. DRACO walking and ATLAS turning with the trained policy: (a) and (e) snapshots of DRACO walking and ATLAS turning. (b) sagittal directional phase plot for the CoM with the SM. (c) LIPM states at the Apex Moment are regulated inside the safety region. (d) yaw angle measurement of the torso along the time axis within the SM.

hardware, DRACO. We have observed many behaviors that the LIPM could not capture and the need for cumbersome tuning procedures in the past. We believe the policy learning technique presented here will automatically determine the gap between model and reality and adjust the policy accordingly.

ACKNOWLEDGMENT

This work was supported by the Office of Naval Research, ONR Grant #N000141512507 and the National Science Foundation, NSF Grant #1724360.

REFERENCES

- [1] Kuindersma *et al.*, “Optimization-based locomotion planning, estimation, and control design for the atlas humanoid robot,” *Autonomous Robots*, vol. 40, no. 3, pp. 429–455, Mar 2016.
- [2] Rezazadeh *et al.*, “Spring-Mass Walking With ATRIAS in 3D: Robust Gait Control Spanning Zero to 4.3 KPH on a Heavily Underactuated Bipedal Robot,” in *ASME 2015 Dynamic Systems and Control Conference*. Columbus: ASME, Oct. 2015, p. V001T04A003.
- [3] S. Caron, A. Kheddar, and O. Tempier, “Stair climbing stabilization of the HRP-4 humanoid robot using whole-body admittance control,” in *IEEE International Conference on Robotics and Automation*, May 2019.
- [4] S. Kajita, F. Kanehiro, K. Kaneko, K. Fujiwara, K. Harada, K. Yokoi, and H. Hirukawa, “Biped walking pattern generation by using preview control of zero-moment point,” in *2003 IEEE International Conference on Robotics and Automation*, vol. 2, Sep. 2003, pp. 1620–1626 vol.2.
- [5] J. Carpentier and N. Mansard, “Multicontact locomotion of legged robots,” *IEEE Transactions on Robotics*, vol. 34, no. 6, pp. 1441–1460, Dec 2018.
- [6] A. Herzog, S. Schaal, and L. Righetti, “Structured contact force optimization for kino-dynamic motion generation,” in *2016 IEEE/RSJ International Conference on Intelligent Robots and Systems (IROS)*, Oct 2016, pp. 2703–2710.

- [7] D. E. Orin, A. Goswami, and S.-H. Lee, “Centroidal dynamics of a humanoid robot,” *Autonomous Robots*, vol. 35, no. 2, pp. 161–176, Oct 2013. [Online]. Available: <https://doi.org/10.1007/s10514-013-9341-4>
- [8] D. Kim, S. J. Jorgensen, J. Lee, J. Ahn, J. Luo, and L. Sentis, “Dynamic locomotion for passive-ankle biped robots and humanoids using whole-body locomotion control,” *arXiv preprint arXiv:1901.08100*, 2019.
- [9] J. Ahn, D. Kim, S. Bang, and L. Sentis, “Control of A High Performance Bipedal Robot using Liquid Cooled Viscoelastic Actuators,” *arXiv preprint arXiv:1906.03811*, 2019.
- [10] Heess *et al.*, “Emergence of locomotion behaviours in rich environments,” *arXiv preprint arXiv:1707.02286*, 2017.
- [11] X. B. Peng, G. Berseth, K. Yin, and M. van de Panne, “Deeploco: Dynamic locomotion skills using hierarchical deep reinforcement learning,” *ACM Transactions on Graphics*, vol. 36, no. 4, 2017.
- [12] S. Levine and V. Koltun, “Guided policy search,” in *Proceedings of the 30th International Conference on Machine Learning*, ser. Proceedings of Machine Learning Research, vol. 28, no. 3, 17–19 Jun 2013, pp. 1–9.
- [13] A. Nagabandi, G. Kahn, R. S. Fearing, and S. Levine, “Neural network dynamics for model-based deep reinforcement learning with model-free fine-tuning,” in *2018 IEEE International Conference on Robotics and Automation (ICRA)*. IEEE, 2018, pp. 7559–7566.
- [14] T. Kurutach, I. Clavera, Y. Duan, A. Tamar, and P. Abbeel, “Model-ensemble trust-region policy optimization,” *arXiv preprint arXiv:1802.10592*, 2018.
- [15] P. Pastor, M. Kalakrishnan, J. Binney, J. Kelly, L. Righetti, G. Sukhatme, and S. Schaal, “Learning task error models for manipulation,” in *2013 IEEE International Conference on Robotics and Automation*, May 2013, pp. 2612–2618.
- [16] R. Cheng, G. Orosz, R. M. Murray, and J. W. Burdick, “End-to-end safe reinforcement learning through barrier functions for safety-critical continuous control tasks,” *arXiv preprint arXiv:1903.08792*, 2019.
- [17] A. Zeng, S. Song, J. Lee, A. Rodriguez, and T. Funkhouser, “Tossing-bot: Learning to throw arbitrary objects with residual physics,” *arXiv preprint arXiv:1903.11239*, 2019.
- [18] J. Garcia and F. Fernández, “A comprehensive survey on safe reinforcement learning,” *Journal of Machine Learning Research*, vol. 16, no. 1, pp. 1437–1480, 2015.
- [19] J. F. Fisac, A. K. Akametalu, M. N. Zeilinger, S. Kaynama, J. Gillula, and C. J. Tomlin, “A general safety framework for learning-based control in uncertain robotic systems,” *IEEE Transactions on Automatic Control*, vol. 64, no. 7, pp. 2737–2752, July 2019.
- [20] T. Pham, G. De Magistris, and R. Tachibana, “Optlayer - practical constrained optimization for deep reinforcement learning in the real world,” in *2018 IEEE International Conference on Robotics and Automation (ICRA)*, May 2018, pp. 6236–6243.
- [21] J. Schulman, F. Wolski, P. Dhariwal, A. Radford, and O. Klimov, “Proximal policy optimization algorithms,” *arXiv preprint arXiv:1707.06347*, 2017.
- [22] G. Brockman, V. Cheung, L. Pettersson, J. Schneider, J. Schulman, J. Tang, and W. Zaremba, “Openai gym,” *arXiv preprint arXiv:1606.01540*, 2016.
- [23] W. Yu, G. Turk, and C. K. Liu, “Learning symmetric and low-energy locomotion,” *ACM Trans. Graph.*, vol. 37, no. 4, pp. 144:1–144:12, Jul. 2018.
- [24] J. Ahn, O. Campbell, D. Kim, and L. Sentis, “Fast kinodynamic bipedal locomotion planning with moving obstacles,” in *2018 IEEE/RSJ International Conference on Intelligent Robots and Systems (IROS)*, Oct 2018, pp. 177–184.
- [25] T. Koolen, T. de Boer, J. Rebuta, A. Goswami, and J. Pratt, “Capturability-based analysis and control of legged locomotion, part 1: Theory and application to three simple gait models,” *The International Journal of Robotics Research*, vol. 31, no. 9, pp. 1094–1113, 2012.
- [26] J. Lee, M. X. Grey, S. Ha, T. Kunz, S. Jain, Y. Ye, S. S. Srinivasa, M. Stilman, and C. K. Liu, “Dart: Dynamic animation and robotics toolkit,” *The Journal of Open Source Software*, vol. 3, no. 22, p. 500, 2018.
- [27] M. VUKOBRATOVI and B. BOROVAC, “Zero-moment point thirty five years of its life,” *International Journal of Humanoid Robotics*, vol. 01, no. 01, pp. 157–173, 2004.